

Probing the Spin-Orbit Time Delay of Multiphoton Ionization of Kr by Bicircular Fields

Peipei Ge,¹ Yiqi Fang,¹ Zhenning Guo,¹ Xueyan Ma,¹ Xiaoyang Yu,¹ Meng Han,¹
Chengyin Wu,^{1,2,3} Qihuang Gong,^{1,2,3} and Yunquan Liu^{1,2,3,4,*}

¹*State Key Laboratory for Mesoscopic Physics and Frontiers Science Center for Nano-optoelectronics,
School of Physics, Peking University, Beijing 100871, China*

²*Collaborative Innovation Center of Quantum Matter, Beijing 100871, China*

³*Collaborative Innovation Center of Extreme Optics, Shanxi University, Taiyuan, Shanxi 030006, China*

⁴*Center for Applied Physics and Technology, HEDPS, Peking University, Beijing 100871, China*



(Received 22 January 2021; accepted 6 May 2021; published 4 June 2021)

We study multiphoton ionization of Kr atoms by circular 400-nm laser fields and probe its photoelectron circular dichroism with the weak corotating and counterrotating circular fields at 800 nm. The unusual momentum- and energy-resolved photoelectron circular dichroisms from the ${}^2P_{1/2}$ ionic state are observed as compared with those from ${}^2P_{3/2}$ ionic state. We identify an anomalous ionization enhancement at sidebands related to the ${}^2P_{1/2}$ ionic state on photoelectron momentum distribution when switching the relative helicity of the two fields from corotating to counterrotating. By performing the two-color intensity-continuously-varying experiments and the pump-probe experiment, we find a specific mixed-photon populated resonant transition channel in counterrotating fields that contributes to the ionization enhancement. We then probe the time delay between the two spin-orbit coupled ionic states (${}^2P_{1/2}$ and ${}^2P_{3/2}$) using bicircular fields and reveal that the resonant transition has an insignificant effect on the relative spin-orbit time delay.

DOI: [10.1103/PhysRevLett.126.223001](https://doi.org/10.1103/PhysRevLett.126.223001)

Photoionization of atoms by intense laser pulses paves the way for strong-field physics. Recently, the strong-field ionization by two-color circularly polarized fields has attracted much attention [1–8]. In contrast to the two-color linearly polarized fields, the two-color circular fields provide an additional parameter, i.e., the relative helicity, in controlling and probing the ionization dynamics. For example, by switching the relative helicity of the fields with respect to one another (i.e., corotating vs counterrotating), one can control the multiphoton transition pathways in the ionization process due to the spin-angular momentum selection rules [5]. Besides, the helicity-induced changes by the circular fields, such as the selective ionization of the p orbitals [9,10] or the generation of the ring currents in the ground state of the ion [11], can be probed by a second-color circular light with corotating and counterrotating geometries. In addition, the ionization response of the polarized atoms or the chiral molecules was found to be sensitive to the helicity of the circularly polarized fields [12,13], which has induced extensive studies on the photoelectron circular dichroism (PECD) [14–17].

In the case of two-color photoionization induced by a strong second harmonic 2ω field and a much weaker fundamental ω field, the sideband peaks emerge between adjacent above-threshold-ionization [18] (ATI) peaks. Very recently, two experiments performed around this intensity condition have shown that the formation of sidebands exhibits circular dichroism, i.e., the yields of sidebands

in corotating fields are higher than those in counterrotating fields [19,20]. This is the usual PECD expected in multiphoton ionization of atoms by the two-color circular fields within strong-field theory. Note that in both experiments, Ar atoms have been chosen as the target system. Owing to the small splitting energy of Ar^+ (0.1775 eV), it is hard to resolve the spin-orbit splitting ionic states (${}^2P_{1/2}$ and ${}^2P_{3/2}$) on the momentum or energy spectrum. On the other side, the spin-orbit coupling effect on the time delay in the single-photon limit has been measured using the reconstruction of attosecond beating by interference of two-photon transition approach [21]. The further intriguing question arises: what is the effect of spin-orbit coupling on the PECD and on the intrinsic time delay between the coupled channels in multiphoton ionization regime?

In this Letter, we experimentally study multiphoton ionization of Kr atoms with the two-color (strong 400 nm + weak 800 nm) circularly polarized fields. Here, we clearly resolve the ATIs and their corresponding sidebands associated with the spin-orbit splitting states (${}^2P_{1/2}$ and ${}^2P_{3/2}$) of Kr^+ on photoelectron momentum distributions (PMDs). Switching the relative helicity of the two colors from corotating to counterrotating, we observe an anomalous ionization enhancement at the sidebands related to the ${}^2P_{1/2}$ state on PMDs. The measured PECD of the ${}^2P_{1/2}$ ionization channel is very different from that of ${}^2P_{3/2}$ ionization channel, and cannot be reproduced by the strong-field approximation (SFA) model [22] and

the solution of time-dependent Schrödinger equation (TDSE) [23] within single-active electron approximation. By performing the two-color intensity-varying and pump-probe experiments, we directly verify that the emerged ionization enhancement results from a photon-spin-allowed resonant transition, and the intermediate state is populated by absorbing mixed-color photons from counterrotating fields. Further, we measure the time delay between the two spin-orbit splitting channels, and find the populated resonant state has an insignificant effect on the relative spin-orbit time delay.

Experimentally, the fundamental field (800 nm, 25 fs, 3 kHz), generated from a Ti:sapphire laser system, is frequency doubled with a 250- μm -thick β -barium-borate crystal to produce its second harmonic (400 nm). The two color pulses are arranged in a Mach-Zehnder interferometer scheme. In each beam, a $\lambda/2$ plate, a thin-film polarizer and a $\lambda/4$ plate are sequentially installed. The circular polarization and the helicity are controlled by rotating the $\lambda/4$ plate relative to the thin-film polarizer. And the laser intensity can be monitored by rotating a $\lambda/2$ plate installed in motorized rotary stage. The two color pulses are temporally overlapped and the relative phase ϕ is finely adjusted by a pair of fused silicon wedges. We focus the two-color circular pulses onto the supersonic gas jet of Kr atoms by a silver concave mirror. The ions and photoelectrons are detected by two separate time- and position-sensitive microchannel plate detectors of cold-target recoil ion momentum spectroscopy [24]. The photoelectron momenta are reconstructed according to the time-of-flight and hitting position. The field intensity is calibrated by comparing the measured photoelectron energy spectrum with the SFA calculation.

Because of the spin-orbit coupling, when a valence electron of the rare gas atom is removed via multiphoton ionization, the p orbitals are no longer degenerated. And the photoelectron energy spectrum would exhibit two sets of ATI peaks corresponding to the ${}^2P_{3/2}$ and ${}^2P_{1/2}$ ionic states. For Kr atoms, the splitting energy is 0.67 eV. In Fig. 1(a), we show the measured PMD of the Kr atoms in the polarization plane (x, z) exposed to the single 400-nm circular field at the intensity of $5.6 \times 10^{13} \text{ W/cm}^2$. One can observe two sets of ATI rings emerge on the PMD. Because the ionization rate strongly depends on the ionization threshold I_p , the photoelectron yields related to ${}^2P_{3/2}$ state ($I_p = 13.99 \text{ eV}$) are generally higher than that of ${}^2P_{1/2}$ ionic state ($I_p = 14.67 \text{ eV}$).

Then, we introduce a weak probing 800-nm circular field ($I_{800} = 1.75 \times 10^{12} \text{ W/cm}^2$) to the ionizing field. By changing the helicity of the 800-nm field, we obtain the phase-integrated PMDs in the polarization plane (x, z) of two-color corotating and counterrotating circular fields, as shown in Figs. 1(b) and 1(c), respectively. Comparing to the PMD in single 400-nm field, one can see two sets of sideband peaks arise between the adjacent ATI peaks in

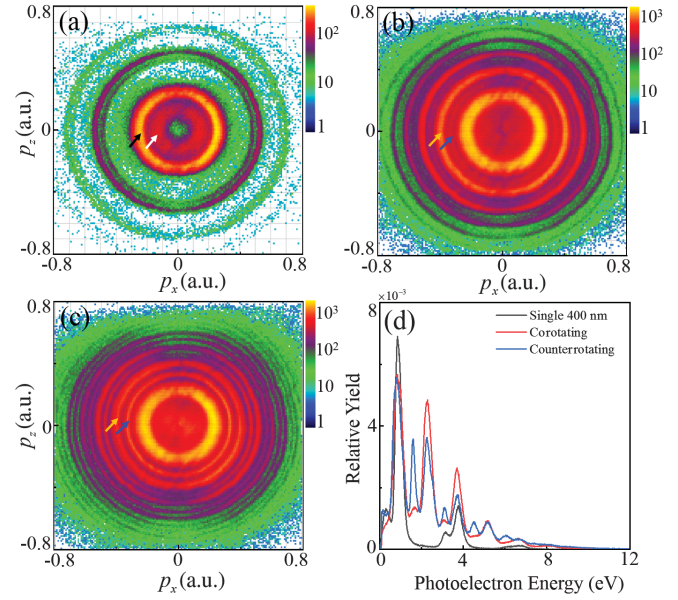


FIG. 1. The experimentally measured photoelectron momentum distributions of Kr on the polarization plane (x, z) in (a) single 400-nm field, the two-color (b) corotating and (c) counterrotating circular fields. The counts are in logarithmic units. (d) The corresponding photoelectron energy spectra for these three fields. The relative yield is obtained by dividing the measured spectrum by its total photoelectron counts. The intensity of 400 nm is fixed to be $5.6 \times 10^{13} \text{ W/cm}^2$. The intensity of 800-nm circular field keeps unchanged ($I_{800} = 1.75 \times 10^{12} \text{ W/cm}^2$) when switching its helicity from corotating to counterrotating. The black (white) and yellow (blue) arrows indicate the first-order ATI peak and sideband related to the spin-orbit splitting state ${}^2P_{3/2}$ (${}^2P_{1/2}$) of Kr^+ , respectively.

two-color bicircular fields. Most surprisingly, we observe the ionization yields at the sidebands of the ${}^2P_{1/2}$ ionization channel are significantly enhanced in counterrotating fields in contrast to the corotating fields. This contradicts the previous observation [19,20], where the sidebands in corotating case were usually much more intense than those in counterrotating case.

For better visibility, we show the phase-integrated photoelectron energy spectra in Fig. 1(d). Because the fundamental field is very weak, the helicity dependence of ac-Stark shift [15] is not evident in the experiment. Apparently, one can see in corotating field the photoelectron yields of the ATIs and sidebands related to ${}^2P_{3/2}$ ionic state are much higher than those of ${}^2P_{1/2}$ ionization channel. This is reasonable because of the lower ionization potential of ${}^2P_{3/2}$ ionic state. However, it is not the case for the counterrotating fields. The yield of photoelectrons from ${}^2P_{1/2}$ channel has been greatly enhanced, especially for the sideband structures. Even their yields are comparable to those of ${}^2P_{3/2}$ sidebands. Such abnormal enhancement would lead to distinct circular dichroisms when comparing the measured PMDs or energy spectra between corotating and counterrotating cases.

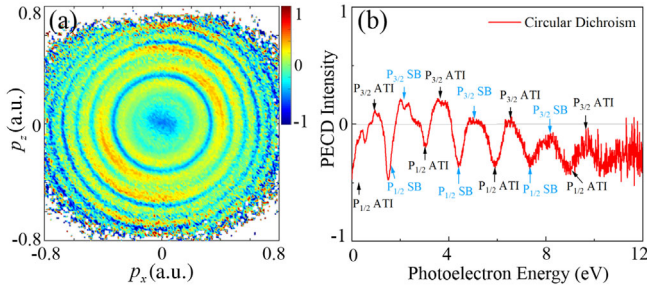


FIG. 2. The measured (a) momentum- and (b) energy-resolved PECDs. The electrons associated with the $2P_{1/2}$ and $2P_{3/2}$ ionic states are indicated by arrows in (b).

Figures 2(a) and 2(b) illustrate the momentum- and energy-resolved PECDs calculated by $[Y_{\text{co}} - Y_{\text{cr}}]/[Y_{\text{co}} + Y_{\text{cr}}]$. Here $Y_{\text{co(cr)}}$ represents the photoelectron yields in corotating (counterrotating) fields. From the measured PECDs, one can see the sign of the PECD alternates as the photoelectron momentum or energy increases. A close inspection shows that the signs of PECD between the $2P_{1/2}$ and $2P_{3/2}$ ionization channels are nearly opposite. For $2P_{3/2}$ ionization channel, the PECD is positive both for ATIs and for sidebands. This means the electrons related to $2P_{3/2}$ state prefer emitting in corotating fields rather than in counterrotating fields. And the PECD intensity slightly decreases with increasing the photoelectron energy. While for $2P_{1/2}$ ionization channel, the sign of PECD is negative, indicating the ionization in counterrotating fields is enhanced. Moreover, the PECD intensity is generally higher than that of $2P_{3/2}$ ionization channel, especially for the sidebands.

To understand the measured PECD, we resort to the simulation using SFA model [22] and the solution of TDSE [23] within single-active electron approximation. The details of the theoretical models and the corresponding results are included in the Supplemental Material [25]. Figure 3 shows the calculated momentum- and energy-resolved PECDs using the SFA model [Figs. 3(a) and 3(b)] and the TDSE method [Figs. 3(c) and 3(d)]. Both calculations show that the PECD of $2P_{1/2}$ ionization channel keeps the same sign with that of $2P_{3/2}$. Neither of them reproduces the measured PECDs of $2P_{1/2}$ ionization channel. The PECD oscillates with increasing the photoelectron energy, and reaches the maximum at sidebands but minimum at ATIs. Specifically, at higher energies, the PECD becomes positive, which means the ionization yields in corotating fields are higher than counterrotating fields. This is very different from the measurement. As for the PECD in the low-energy region, there exists large discrepancies between the two calculations, which is associated with the ignorance of the Coulomb potential in SFA model.

The single-active-electron models fail to reproduce the anomalous PECD of $2P_{1/2}$ ionization channel. Thus, the resonant enhancement in counterrotating fields is expected to be crucial. To verify this conjecture, we then performed the intensity-varying experiments with two-color circular

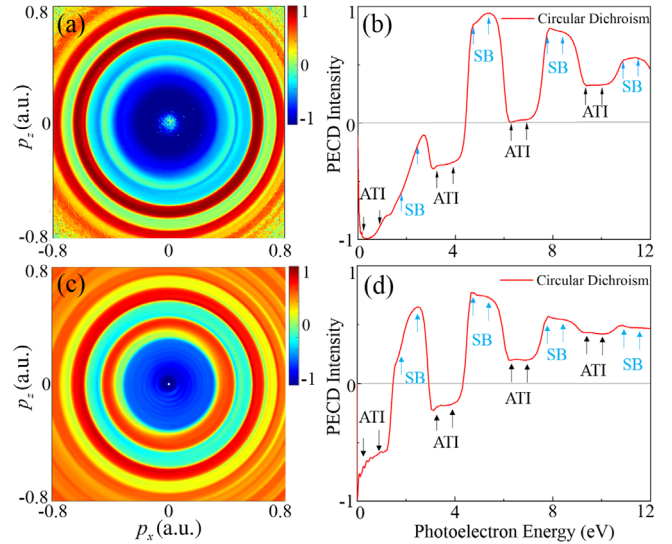


FIG. 3. The calculated (a) momentum- and (b) energy-resolved PECDs by the SFA model. (c), (d) The corresponding results calculated by the TDSE method. The energy positions of the ATIs and sidebands associated with the $2P_{1/2}$ and $2P_{3/2}$ states are indicated by arrows in (b) and (d).

fields. Because the resonant ionization channel is laser-intensity-independent [26], one can clearly distinguish it from the intensity-dependent photoelectron energy distributions. Here, the intensity of 400-nm field is continuously changed, while the intensity of 800 nm remains unchanged at 1.75×10^{12} W/cm². Figures 4(a) and 4(b) show the measured intensity-dependent photoelectron energy distributions in corotating and counterrotating fields, respectively. One can see the yields of $2P_{3/2}$ sidebands in corotating fields are generally higher than those in counterrotating fields, but it is not the case for $2P_{1/2}$ channel. Apart from the intensity-dependent energy peaks, we observe a prominent intensity-independent structure located at ~ 1.5 eV in counterrotating fields, which coincides with the first-order sideband of $2P_{1/2}$ ionization channel. Such intensity independence persists in high-order $2P_{1/2}$ sidebands. This phenomenon indicates that the observed ionization enhancement at $2P_{1/2}$ sidebands in counterrotating fields originates from a resonant ionization channel, and such resonant transition is absent in corotating fields. Because the laser intensity of 400 nm is changed continuously, one can exclude the possibility that the helicity-dependent ac-Stark shift results in the discrepancy. A possible mechanism is that the probing 800-nm field participates in the resonant transition. As known, the circularly polarized field with different helicity would have different spin-angular momentum. If the electron absorbs photons with different spin, it will transit into different intermediate state due to the spin-angular momentum selection rules.

To further support the above explanation, we have performed the pump-probe experiments with the two-color

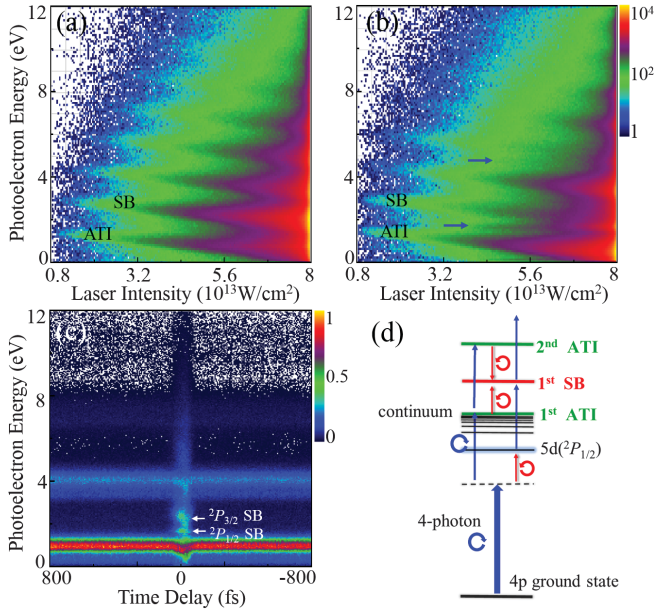


FIG. 4. The measured laser-intensity-dependent photoelectron energy distributions in two-color (a) corotating and (b) counterrotating fields. The blue arrow in (b) indicates the energy of emerged resonant ionization channel located at the sidebands related to the $^2P_{1/2}$ ionic state without the laser intensity dependence. (c) The measured photoelectron energy distribution in the pump-probe experiment with two-color counterrotating fields. The positive (negative) time delay represents that the strong 400-nm circular pulse proceeds (lags behind) the weak 800-nm circular pulse. (d) The schematic illustration of the involved multiphoton transitions for $^2P_{1/2}$ ionic state in counterrotating fields.

counterrotating circular fields. We keep the intensities of the two-color pulses the same with the former experiments as in Figs. 1. And we use the motorized displacement stage placed in the 800-nm arm to control the pump-probe time delay. Figure 4(c) shows the time-resolved photoelectron energy distribution in the counterrotating fields. The positive (negative) time delay means the strong 400-nm circular field proceeds (lags behind) the weak 800-nm circular field. One can see at the temporal region when the two pulses are not overlapping, the energy distribution exhibits distinct the 400-nm ATI peaks. No ionization contribution from the excited states populated by either field is probed. While at the overlapping region, besides the emergence of sidebands, we do observe the ionization enhancement occurs with the energy coinciding with $^2P_{1/2}$ sidebands. The pump-probe experiment directly indicates that the ionization enhancement in counterrotating fields happens only when the two fields are overlapped in time. In other words, this means the involved resonant transition is facilitated by absorption of mixed photons with opposite helicities (or photon spins).

In the experiment, the circular 800-nm field is too weak and cannot induce ionization solely, thus we infer that only

one 800-nm photon has been involved in the transition process. As illustrated in Fig. 4(d), the 4p ground-state electron of Kr atom first absorbs four 400-nm circular photons together with a counterrotating 800-nm photon, then it comes into resonance with an intermediate state. Afterwards, the excited electrons prefer to absorbing the 400-nm photons from the two-color fields to be ionized because of the strong intensity of the 400-nm fields. This enables the ATI process from the intermediate state and the energies of the released photoelectrons coincide with the ordinary $^2P_{1/2}$ sidebands. While in the corotating fields, the transition is forbidden because of the spin-angular momentum selection rules. According to the selection rules, the photoelectron energy and the energy levels of Kr atom [27], we can identify the involved intermediate state as the ($^2P_{1/2}$) 5d state with $m = 2, J = 1, 2; 2, 3$, here J is the total angular momentum [25].

As we have resolved the spin-orbit coupled channels of Kr on the PMD, we then further investigate the intrinsic spin-orbit delay in multiphoton regime using the two-color bicircular fields. It would be certain interesting for the measurement when a new resonant ionization channel has contributed to $^2P_{1/2}$ sidebands in counterrotating fields. We can take $^2P_{3/2}$ sidebands as a reference to investigate the influence of the resonant transition on the delay. Figures 5(a) and 5(b) show the phase-resolved p_z distributions in corotating and counterrotating fields. The delay

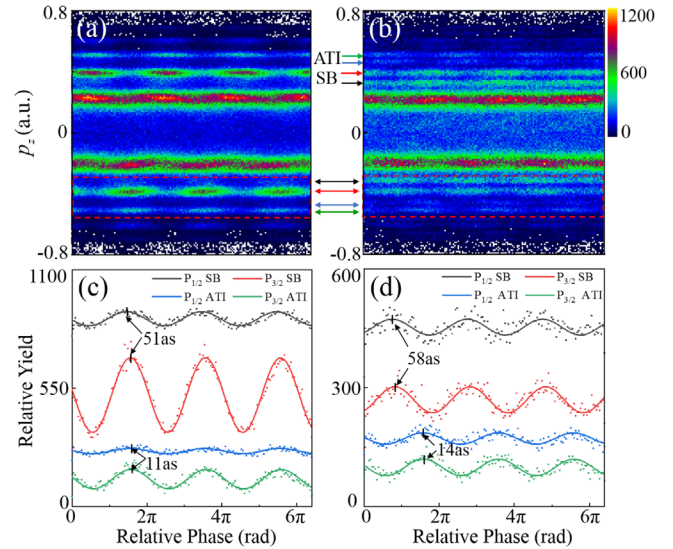


FIG. 5. (a),(b) The extracted phase-resolved photoelectron momentum distributions from Figs. 1(b) and 1(c) along the p_z direction ($|p_x| < 0.05$ a.u.) in corotating and counterrotating fields. The positions of the first-order sidebands and second-order ATIs for $^2P_{1/2}$ and $^2P_{3/2}$ channels are guided by black, red, blue, and green arrows, respectively. (c),(d) The extracted photoelectron yield oscillations of different ionization channels from the dashed square region in (a) and (b). The vertical short lines mark the positions of the yield maxima. The relative time delays are labeled.

information can be extracted from the phase difference between the photoelectron yield oscillations [28].

As shown in Figs. 5(c) and 5(d), we present the photoelectron yield oscillations of ${}^2P_{1/2}$ and ${}^2P_{3/2}$ ionization channels in the $-z$ half plane for corotating and counterrotating cases. Each yield oscillation is fitted with a cosine function $Y = A \cos(\phi + \varphi)$ [29], where $\phi = 2\omega t$ represents the relative phase between the two colors. And the relative delay can be extracted with $\Delta\tau = (\varphi_1 - \varphi_2)/2\omega$. Focusing on the first-order sidebands of ${}^2P_{1/2}$ and ${}^2P_{3/2}$ ionization channels, we reveal a “spin-orbit delay” of 51 *as* in the corotating case while 58 *as* in counterrotating case. Compared with the previous measurement [21], where the measured spin-orbit delay is smaller than 8 *as*, the larger time delays in our experiment can be attributed to the contribution of the continuum-continuum delay [30] (i.e., τ_{cc}), which strongly depends on the photoelectron energy. With the increasing of the photoelectron energy, the contribution from τ_{cc} will be reduced and a smaller spin-orbit delay would be obtained. This can be verified by the spin-orbit delays extracted from the second-order ATIs, i.e., 11 *as* and 14 *as* in co- and counterrotating fields, as seen in Fig. 5. Considering the inhomogeneous detection efficiency of the detector and the errors in fitting process, the spin-orbit delays extracted from other emission angle slightly differ within ± 2 *as*. Note that the extracted time delays in corotating and counterrotating cases are very close, indicating that the emerged resonant ionization channel in counterrotating fields has a relatively small effect on time delay. This differs from the previous measurements, where the resonant state populated by the single-color photons can induce much larger time (phase) shift [31,32].

In conclusion, we experimentally investigate multiphoton ionization of Kr atoms with the evident spin-orbit coupling effect in two-color corotating and counterrotating circular pulses. The high-resolution PMD shows distinct circular dichroisms when switching the relative helicity of the two colors from corotating to counterrotating. An enhancement at the sidebands from the ${}^2P_{1/2}$ state is observed, which is essentially different from the normal PECDs measured in [19,20]. Our experiment indicates the photon spin (or the light helicity) plays a very important role in the PECD with two-color circular fields. Similar mechanism has been observed in high-order harmonic generation by two-color counterrotating circular fields [33]. Recently, the PECD was used to control the energy transfer in multiphoton ionization [34]. The measured unusual PECD in our experiment lacks of the dedicated theoretical explanation. The modeling of the real multi-electron atoms is expected.

We further show that the resonant transition has an insignificant effect on the relative photoemission time delay of spin-orbit coupled channels. Note that the effects of long-range Coulomb interaction, nonadiabaticity, polarization, or

multielectrons cannot be decoupled on the time delay of the spin-orbit coupled channels, which needs more sophisticated investigation in the future. This study has potential implications for monitoring the photoelectron spin polarization with two-color circularly polarized fields and would also facilitate the integrated studies of the spin-orbit interaction between electrons and photons in strong-field regime [35,36]. The ionization associated with the ${}^2P_{1/2}$ state can yield the photoelectrons with high spin-polarization [37–40]. Thus, it would be very interesting to learn the information of spin polarization of ATIs and sidebands of the ${}^2P_{1/2}$ channel using bicircular fields in the future.

This work is supported by the National Natural Science Foundation of China (Grants No. 92050201, No. 11774013, No. 11527901, and No. 11625414).

*Corresponding author.

yunquan.liu@pku.edu.cn

- [1] C. A. Mancuso, D. D. Hickstein, P. Grychtol, R. Knut, O. Kfir *et al.*, *Phys. Rev. A* **91**, 031402(R) (2015).
- [2] C. A. Mancuso, D. D. Hickstein, K. M. Dorney, J. L. Ellis, E. Hasović *et al.*, *Phys. Rev. A* **93**, 053406 (2016).
- [3] C. A. Mancuso, K. M. Dorney, D. D. Hickstein, J. L. Chaloupka, J. L. Ellis, F. J. Dollar, R. Knut, P. Grychtol, D. Zusin, C. Gentry, M. Gopalakrishnan, H. C. Kapteyn, and M. M. Murnane, *Phys. Rev. Lett.* **117**, 133201 (2016).
- [4] S. Eckart *et al.*, *Phys. Rev. Lett.* **117**, 133202 (2016).
- [5] C. A. Mancuso, K. M. Dorney, D. D. Hickstein, J. L. Chaloupka, X. M. Tong, J. L. Ellis, H. C. Kapteyn, and M. M. Murnane, *Phys. Rev. A* **96**, 023402 (2017).
- [6] S. Eckart, K. Fehre, N. Eicke, A. Hartung, J. Rist, D. Trabert, N. Strenger, A. Pier, L. Ph. H. Schmidt, T. Jahnke, M. S. Schöffler, M. Lein, M. Kunitski, and R. Dörner, *Phys. Rev. Lett.* **121**, 163202 (2018).
- [7] M. Han, P. Ge, Y. Shao, Q. Gong, and Y. Liu, *Phys. Rev. Lett.* **120**, 073202 (2018).
- [8] P. Ge, M. Han, Y. Deng, Q. Gong, and Y. Liu, *Phys. Rev. Lett.* **122**, 013201 (2019).
- [9] I. Barth and O. Smirnova, *Phys. Rev. A* **84**, 063415 (2011); **87**, 013433 (2013).
- [10] T. Herath, L. Yan, S. K. Lee, and W. Li, *Phys. Rev. Lett.* **109**, 043004 (2012).
- [11] S. Eckart *et al.*, *Nat. Phys.* **14**, 701 (2018).
- [12] P. Lambropoulos, *Phys. Rev. Lett.* **28**, 585 (1972).
- [13] N. Böwering, T. Lischke, B. Schmidtke, N. Müller, T. Khalil, and U. Heinzmann, *Phys. Rev. Lett.* **86**, 1187 (2001).
- [14] T. Mazza *et al.*, *Nat. Commun.* **5**, 3648 (2014).
- [15] M. Ilchen, N. Douguet, T. Mazza, A. J. Rafipoor, C. Callegari *et al.*, *Phys. Rev. Lett.* **118**, 013002 (2017).
- [16] C. Lux, M. Wollenhaupt, T. Bolze, Q. Liang, J. Köhler, C. Sarpe, and T. Baumert, *Angew. Chem., Int. Ed. Engl.* **51**, 5001 (2012).
- [17] C. S. Lehmann, N. B. Ram, I. Powis, and M. H. M. Janssen, *J. Chem. Phys.* **139**, 234307 (2013).

- [18] P. Agostini, F. Fabre, G. Mainfray, G. Petite, and N. K. Rahman, *Phys. Rev. Lett.* **42**, 1127 (1979).
- [19] M. Han, P. Ge, Y. Fang, X. Yu, Z. Guo, Y. Deng, Q. Gong, and Y. Liu, *Phys. Rev. A* **101**, 043406 (2020); M. Han, H. Liang, P. Ge, Y. Fang, Z. Guo, X. Yu, Y. Deng, L. Y. Peng, Q. Gong, and Y. Liu, *Phys. Rev. A* **102**, 061101(R) (2020).
- [20] S. Eckart, D. Trabert, K. Fehre, A. Geyer, J. Rist, K. Lin, F. Trinter, L. Ph. H. Schmidt, M. S. Schöffler, T. Jahnke, M. Kunitski, and R. Dörner, *Phys. Rev. A* **102**, 043115 (2020).
- [21] I. Jordan, M. Huppert, S. Pabst, A. S. Kheifets, D. Baykusheva, and H. J. Wörner, *Phys. Rev. A* **95**, 013404 (2017).
- [22] F. H. M. Faisal, *J. Phys. B* **6**, L89 (1973); H. Reiss, *Phys. Rev. A* **22**, 1786 (1980).
- [23] V. Mosert and D. Bauer, *Comput. Phys. Commun.* **207**, 452 (2016).
- [24] J. Ullrich, R. Moshhammer, A. Dorn, R. Dörner, L. Ph. H. Schmidt, and H. Schmidt-Böcking, *Rep. Prog. Phys.* **66**, 1463 (2003).
- [25] See Supplemental Material at <http://link.aps.org/supplemental/10.1103/PhysRevLett.126.223001> for the theoretical models and the corresponding results, and the determination of the resonant state.
- [26] Q. Li, X. M. Tong, T. Morishita, H. Wei, and C. D. Lin, *Phys. Rev. A* **89**, 023421 (2014).
- [27] <https://physics.nist.gov/cgi-bin/ASD/energy1.pl>.
- [28] L. J. Zipp, A. Natan, and P. H. Buchsbaum, *Optica* **1**, 361 (2014).
- [29] P. M. Paul, E. S. Toma, P. Breger, G. Mullot, F. Augé, Ph. Balcou, H. G. Muller, and P. Agostini, *Science* **292**, 1689 (2001).
- [30] J. M. Dahlström, D. Guénot, K. Klünder, M. Gisselbrecht, J. Mauritsson, A. L'Huillier, A. Maquet, and R. Taëb, *Chem. Phys.* **414**, 53 (2013).
- [31] M. Swoboda, T. Fordell, K. Klünder, J. M. Dahlström, M. Miranda, C. Buth, K. J. Schafer, J. Mauritsson, A. L'Huillier, and M. Gisselbrecht, *Phys. Rev. Lett.* **104**, 103003 (2010).
- [32] J. Su, H. Ni, A. Jaroń-Becker, and A. Becker, *Phys. Rev. Lett.* **113**, 263002 (2014).
- [33] G. Dixit, Á. Jiménez-Galán, L. Medišauskas, and M. Ivanov, *Phys. Rev. A* **98**, 053402 (2018).
- [34] A. H. N. C. De Silva *et al.*, *Phys. Rev. Lett.* **126**, 023201 (2021).
- [35] M. Han, P. Ge, Y. Fang, X. Yu, Z. Guo, Y. Deng, C. Wu, Q. Gong, and Y. Liu, *Phys. Rev. A* **101**, 061401(R) (2020).
- [36] Y. Fang, M. Han, P. Ge, Z. Guo, X. Yu, Y. Deng, C. Wu, Q. Gong, and Y. Liu, *Nat. Photonics* **15**, 115 (2021).
- [37] I. Barth and O. Smirnova, *Phys. Rev. A* **88**, 013401 (2013).
- [38] A. Hartung *et al.*, *Nat. Photonics* **10**, 526 (2016).
- [39] M. M. Liu, Y. Shao, M. Han, P. Ge, Y. Deng, C. Wu, Q. Gong, and Y. Liu, *Phys. Rev. Lett.* **120**, 043201 (2018).
- [40] D. Trabert, A. Hartung, S. Eckart, F. Trinter, A. Kalinin, M. Schöffler, L. Ph. H. Schmidt, T. Jahnke, M. Kunitski, and R. Dörner, *Phys. Rev. Lett.* **120**, 043202 (2018).